CMS Physics Analysis Summary

Contact: cms-pag-conveners-exotica@cern.ch 2017/12/12

Search for lepton flavour violating decays of heavy resonances and quantum black holes to eμ pairs in proton-proton collisions at $\sqrt{s} = 13$ TeV

The CMS Collaboration

Abstract

A search is reported for heavy resonances decaying into eμ final states using proton-proton collision data recorded by the CMS experiment at the CERN LHC at $\sqrt{s} =$ 13 TeV, corresponding to an integrated luminosity of 35.9 fb^{-1}. The search focuses on resonance masses above 200 GeV. With no evidence found for physics beyond the standard model in the mass spectrum of selected eμ pairs, upper limits are set at the 95% confidence level on the product of the cross section and branching fraction for signals in models that incorporate lepton-flavour violation in interactions of charged leptons. Resonant τ sneutrino production in R-parity violating supersymmetry is excluded for τ sneutrino masses below 1.7 TeV, and couplings $\lambda_{132} = \lambda_{231} = \lambda'_{311} = 0.01$. Heavy Z′ gauge bosons in lepton flavour violating transitions are excluded up to 4.4 TeV. The eμ mass spectrum is also interpreted in terms of a non-resonant contribution from quantum black hole production in models with extra spatial dimensions. The exclusion limits range from 3.6 TeV to 5.6 TeV for number of extra dimensions between one and six.

1 Introduction

Several extensions of the standard model (SM) predict the existence of heavy particles that undergo lepton flavor violating (LFV) decays, thereby motivating searches for deviations from the SM in the eμ final state. This note reports a search for phenomena beyond the SM in the invariant mass spectrum of eμ pairs ($m_{e\mu}$). The analysis is based on data corresponding to an integrated luminosity of 35.9 fb^{-1} collected in the year 2016 in proton-proton (pp) collisions at $\sqrt{s} = 13$ TeV in the CMS detector at the CERN LHC. The results are interpreted in terms of the characteristics of the following predicted objects: a τ sneutrino ($\tilde{\nu}_\tau$) — the lightest supersymmetric particle (LSP) in R-parity violating (RPV) supersymmetry (SUSY) [1], a heavy Z′ gauge boson in LFV models [2], and quantum black holes (QBH) [3, 4].

In RPV SUSY, lepton flavour and lepton number are violated at lowest Born level in interactions between fermions and their superpartners, where the $\tilde{\nu}_\tau$ is the LSP. For resonant $\tilde{\nu}_\tau$ signals, the trilinear RPV part of the superpotential can be expressed as: $W_{\mathrm{RPV}} = \frac{1}{2}\lambda_{ijk} L_i L_j \bar{E}_k + \lambda'_{ijk} L_i Q_j \bar{D}_k$ ($i, j, k \in 1, 2, 3$), where i, j and k are generation indices, L, and Q are the $\mathrm{SU}(2)_L$ doublet superfields of the leptons and quarks, and $\bar{E}$ and $\bar{D}$ are the $SU(2)_L$ singlet superfields of the charged leptons and down-like quarks. We suppose that all RPV couplings vanish, except for λ_{132}, λ_{231} (called λ), and λ'_{311} (called λ'), which are connected to the production and decay of the $\tilde{\nu}_\tau$, and we consider a SUSY mass hierarchy with $\tilde{\nu}_\tau$ as the LSP. In this model, the $\tilde{\nu}_\tau$ can be produced resonantly in pp collisions via the λ'_{311} coupling, and decays either into an eμ pair via the λ_{132} and λ_{231} couplings, or into a d$\bar{\mathrm{d}}$ pair via the λ'_{311} coupling. We consider only the eμ final state, and assume $\lambda_{132} = \lambda_{231}$. In this analysis, only prompt decays of the $\tilde{\nu}_\tau$ are considered and not long-lived $\tilde{\nu}_\tau$ decays that would provide displaced eμ pairs.

An extension of the SM through the addition of an extra U(1) gauge symmetry provides a massive Z′ vector boson [2]. In this search, we assume that the Z′ boson has couplings similar to the Z boson in the SM, but the Z′ can decay to the LFV eμ final state with a branching fraction of 10%, which provides a relatively constant width to mass ratio of $\approx 3\,\%$ for the Z′ boson.

Theories that invoke extra spatial dimensions offer fundamental Planck scales in the TeV region. Such theories also provide the possibility of producing microscopic black holes [3, 4] at the LHC. In contrast to semiclassical, thermal black holes, which would decay to high-multiplicity final states, QBH are nonthermal objects, expected to decay predominantly to pairs of particles. We consider the production of a spin-0, colourless, neutral QBH in a model with LFV [5], in which the cross section for QBH production depends on the threshold mass m_{th} for QBH production in n additional spatial dimensions. The case $n = 1$ corresponds to the Randall–Sundrum (RS) brane world model [6], and $n > 1$ corresponds to the Arkani-Hamed–Dimopoulos–Dvali (ADD) model [7]. While the resonant $\tilde{\nu}_\tau$ and Z′ signals generate narrow peaks in the mass spectrum of the eμ pair, the mass distribution of the QBH signal is characterized by a ledge at the threshold of QBH production, followed by a monotonic fall off.

Searches similar to this one have been carried out by the CDF [8] and D0 [9] Collaborations at the Fermilab Tevatron in p$\bar{\mathrm{p}}$ collisions at a centre-of-mass energy of 1.96 TeV and by the ATLAS and CMS Collaborations at the LHC in pp collisions at a centre-of-mass energy of 8 TeV [10, 11] and 13 TeV [12]. The search at CMS at 8 TeV makes use of an integrated luminosity of 19.7 fb^{-1} to exclude τ sneutrino masses up to 1.28 TeV for $\lambda_{132} = \lambda_{231} = \lambda'_{311} = 0.01$. The search performed by ATLAS at 13 TeV with 3.2 fb^{-1} of luminosity excludes Z′ up to $m_{Z'} = 3.01$ TeV. The present search significantly extends these limits.

2 The CMS detector

The central feature of the CMS apparatus is a superconducting solenoid of 6 m internal diameter, providing a magnetic field of 3.8 T. Within the solenoid volume are a silicon pixel and strip tracker, a lead tungstate crystal electromagnetic calorimeter (ECAL), and a brass and scintillator hadron calorimeter (HCAL), each composed of a barrel and two endcap sections. Forward calorimeters extend the pseudorapidity coverage provided by the barrel and endcap detectors. Muons are detected in gas-ionization chambers embedded in the steel flux-return yoke outside the solenoid. A more detailed description of the CMS detector, together with a definition of the coordinate system used and the relevant kinematic variables, can be found in Ref. [13].

3 Event selection

The search is designed to be inclusive and model independent, requiring only a prompt, isolated muon, and a prompt, isolated electron in the event. This minimal selection also facilitates a reinterpretation of the results in terms of models with more complex signal topologies than the single eμ pair. Events that satisfy single-muon (-photon) triggers [14] with transverse momentum (p_{T}) threshold of 50 (175) GeV for muons (photons) are selected for analysis. A photon trigger, instead of electron, is used to trigger on electromagnetic energy deposit expected from the electron. This is because the photon trigger allows looser isolation requirements on the electromagnetic object, which is utilized later to estimate certain types of backgrounds from data itself. Using a photon trigger to select electron is possible because electrons are expected to pass photon triggers also.

Electrons and muons are reconstructed and identified using standard CMS algorithms, described in Refs. [15, 16]. To reconstruct a muon candidate, hits in the inner tracker and in the muon system are first fitted separately to inner-tracker and standalone outer-muon trajectories that are combined in a global-muon track hypothesis. Muon candidates are required to have a transverse momentum (p_{T}) > 53 GeV and to fall into the acceptance region in pseudorapidity ($|\eta|$) < 2.4. The transverse and longitudinal impact parameters of the muon candidate, relative to the primary vertex position, must be less than 0.2 cm and 0.5 cm, respectively. The primary vertex of an event is chosen to be the reconstructed vertex with the largest p_{T}^2 sum of associated tracks. The track of the muon candidate must have at least one hit in the pixel detector, hits in at least six silicon-strip layers, and contain matched segments in at least two muon detector planes. To suppress backgrounds arising from muons within jets, the scalar-p_{T} sum of all other tracks in the tracker within a cone of $\Delta R = \sqrt{(\Delta\eta)^2 + (\Delta\phi)^2} < 0.3$ around the muon candidate track (where $\Delta\phi$ are the differences in azimuth (in radians) between the muon and the other tracks) is required to be less than 10% of the p_{T} of the muon candidate. The relative uncertainty in p_{T} of the muon track is required to be smaller than 30%.

To reconstruct an electron candidate, energy depositions in the ECAL are first combined into clusters, assuming that each cluster represents a single particle. The clusters are then combined in a way consistent with bremsstrahlung emission, to produce a single "supercluster", which represents the electron or photon. These superclusters are used to seed tracking algorithms, and if a resulting track is found, it is associated with the supercluster to form an electron candidate. The electron candidates are required to pass the high-energy electron pairs (HEEP) selection [15], which requires the energy deposition in the ECAL to be consistent with that of an electron. The sum of the energy in the brass and scintillator hadronic calorimeter in a cone of $\Delta R < 0.15$ centred around the electron candidate must be less than 5 % of the electron candidate's energy, after it is corrected for activity unrelated to the electron. The electron candidate

must have a well matched prompt track in the η-ϕ plane that has no more than one hit missing in the inner portion of the tracker. The HEEP selection also requires the electrons to be isolated, the requirement for which is that the scalar-p_T sum of tracks within a cone of radius $\Delta R = 0.3$ around the candidate direction is less than 5 GeV, and the p_T sum of energy depositions within this cone, with small η-dependent offsets, is less than 3 % of the p_T value of the candidate.

To reduce loss in signal efficiency from possible electron charge misidentification at high electron p_T, the electron and muon are not required to have opposite charges. Since highly energetic muons can produce bremsstrahlung and an associated supercluster in the ECAL along the direction of the inner-muon trajectory, they can be misidentified as electrons. An electron candidate is therefore rejected if there is a muon with p_T greater than 5 GeV within $\Delta R < 0.1$ of the electron candidate. Only one eμ pair is considered per event. When there is more than one eμ candidate, in the event, the pair with the highest invariant mass is selected for the analysis.

4 Signal simulation

The RPV SUSY and QBH signal event samples are generated at leading order (LO) precision, using the CALCHEP 3.6 [17] and QBH 2.0 [18] Monte Carlo (MC) event generators respectively. The Z′ signal events are produced at LO using the PYTHIA 8.203 generator [19]. For Z′ signal, the relative decay width is taken as 3 % of the mass. Interference between SM Z and Z′ is not taken into account. All simulated signal and background events use PYTHIA for hadronization and the underlying event tune CUETP8M1 [20]. RPV and QBH signal processes are generated using CTEQ6L [21] parton distribution functions (PDFs) and Z′ signals are generated using NNPDF 3.0 [22] PDF. A cross section calculated at next-to-leading order (NLO) in perturbative quantum chromodynamics (QCD) is used for the RPV signal, in which the factorization and renormalization scales are set to the mass of the τ sneutrino. The generated events are processed through a full simulation of the CMS detector based on GEANT4 [23–25]. The simulated events incorporate additional pp interactions (pileup) within the same or a nearby bunch crossing, which are weighted to match the measured distribution in the number of interactions per bunch crossing. The simulated samples are normalized to the integrated luminosity of the data of 35.9 fb^{-1}. The product of the total acceptance and efficiency for the three signal models used in this analysis is determined using MC simulation. The trigger and object reconstruction efficiencies are corrected to the values measured in data. The selection efficiency for the RPV $\tilde{\nu}_\tau$ signal is $\approx$ 60% at $m_{\tilde{\nu}_\tau} = 1$ TeV and $\approx$ 66% at $m_{\tilde{\nu}_\tau} = 4$ TeV. The selection efficiency for the QBH signal is $\approx$ 60% at $m_{\text{th}} = 1$ TeV and $\approx$ 64% at $m_{\text{th}} = 4$ TeV, and for Z′ signal it is $\approx$ 55% at $m_{Z'} = 1$ TeV and $\approx$ 63% at $m_{Z'} = 4$ TeV.

5 Background estimation

The SM backgrounds contributing to the eμ final state are divided into two categories. The first one comprises events with at least two prompt, isolated leptons while the second category comprises events that include either jets or photons misidentified as isolated leptons; or jets with leptons from heavy-flavour decays, both of which we refer to as non-prompt background.

The expected SM background from processes with two prompt leptons is obtained from MC simulation. It consists mostly of events from $\mathrm{t\bar{t}}$ production and WW production; the former process is dominant at lower masses and the latter becomes equally important above $M_{e\mu} \approx 1$ TeV. Other backgrounds estimated from MC simulation involve the diboson contributions WZ and ZZ; single top quark production; and Drell–Yan (DY) production (i.e. $\mathrm{q\bar{q}} \to$ virtual Z or $\gamma \to$ two leptons of opposite charge) in the ee, $\mu\mu$ and $\tau\tau$ channels. All of these, with the

exception of $\tau\tau$ final states, are generated at NLO using the POWHEG 2.0 [26] event generator, while the DY to $\tau\tau$ background is generated at NLO using the MADGRAPH5_AMC@NLO 2.2.2 [27, 28] event generator. Cross sections for the normalization are calculated at next-to-next-to-leading order accuracy for WW, ZZ, single top quark, and $\mathrm{t\bar{t}}$ processes, and at NLO accuracy for WZ and DY events. All background processes are simulated using the NNPDF 3.0 PDF.

The main sources of nonprompt background in the eμ selection are from W+jets and Wγ production, where a jet or a photon is misidentified as an electron. The Wγ process also contributes to the prompt background category through an internal conversion of γ to leptons. The QCD-multijet process provides subleading contributions to the background with nonprompt leptons. The estimate of the Wγ background is obtained at LO from MC simulation based on the MADGRAPH5_AMC@NLO event generator. A background estimation based on control samples in data, using jet-to-electron misidentification rate (F), is used to determine the $m_{\mathrm{e}\mu}$ distributions from W+jets and multijet contributions. The jet-to-electron misidentification rate is measured in the data, using a control sample collected with a single electromagnetic cluster trigger. Data sidebands are used to evaluate the contributions to the control samples from genuine electrons and photons misidentified as electrons. The jet-to-electron misidentification rate is then defined as the number of electrons passing the full selection divided by the number of electron candidates in the sample. The rate is quantified in bins of p_{T} and η. The measured rate is used to estimate the W+jets and multijet contributions from data containing muons that pass the single-muon trigger and the full muon selection, and electron candidates satisfying relaxed selection requirements, but failing the full electron selection. Each event is weighted by the factor $F/(1-F)$ to determine the overall contribution from the jet backgrounds. Contributions from processes other than W+jets and multijet sources are subtracted from the sample after applying the falsification rate to avoid double counting. This is done using MC simulated background events. Background from jets mimicking muons was estimated to be only 1% of the total background, and it is therefore not taken into account.

6 Systematic uncertainties

Uncertainties in the modelling of the eμ invariant mass are taken into account for the leading $\mathrm{t\bar{t}}$ and subleading WW backgrounds. The $\mathrm{t\bar{t}}$ background provides the dominant uncertainty of no more than 25 % in the total background yield at $m_{\mathrm{e}\mu} \approx 700\,\mathrm{GeV}$. This is estimated from the resummed next-to-next-to-leading-logarithm calculation of the soft-gluon cross section at NLO, as presented in Ref. [29]. The uncertainty on the WW background distribution is estimated to be $\approx$ 2.5% at $m_{\mathrm{e}\mu} \approx 1$ TeV. A systematic uncertainty of 2.5% [30] in the integrated luminosity is used for backgrounds and signals. Among the uncertainties in the cross sections used for the normalization of the various simulated background samples, 5% uncertainty for the dominant $\mathrm{t\bar{t}}$ background is most relevant. The uncertainty in the muon momentum scale depends on η and ϕ of muons and leads to an uncertainty on the total background yield of $\approx$ 1.1% at $m_{\mathrm{e}\mu} = 500\,\mathrm{GeV}$ and $\approx$ 25% at $m_{\mathrm{e}\mu} = 2\,\mathrm{TeV}$. Uncertainty on the muon efficiency scale factor is 2–3% over the whole mass range. Apart from that, a momentum-dependent, downward-only systematic uncertainty is applied on muon reconstruction and identification efficiency to account for the observed trend in data of a smaller number of events than predicted for high-p_{T} muons. This amounts to –1.6% in the region $|\eta| < 1.6$ and –14.4% in the region $1.6 < |\eta| < 2.4$ for muons with momentum of 4 TeV. Uncertainties in the electron p_{T} scale and resolution, muon p_{T} resolution, and pileup have negligible impact on the total background yield. Uncertainty on the electron efficiency scale factor is 2–3% over the whole mass range. The uncertainty associated with the choice of PDF in the simulation is evaluated

according to the PDF4LHC prescription [31, 32]. All these uncertainties are also considered for the signal prediction. A systematic uncertainty of 50% is applied to the estimate of the jet background obtained from data. Taking all systematic uncertainties into account, the resulting uncertainty on the background yield ranges from 15% at $m_{e\mu} = 200\,\text{GeV}$ to 40% at $m_{e\mu} = 2\,\text{TeV}$.

7 Results

The eμ mass distribution for the selected events is shown in Fig. 1, together with the corresponding cumulative (integrated from the chosen $m_{e\mu}$ threshold to infinity) distribution. After selection, 4 events are observed in data in the region $m_{e\mu} > 1.5$ TeV, where the expectation from SM background is 4.2 ± 0.35 (stat) ± 0.91 (syst). The data are consistent within the uncertainties with the SM expectation in the whole mass range. No significant excess is observed relative to the SM expectation in the eμ invariant mass distribution. We set limits on the product of the signal cross section (σ) and the branching fraction of signal (B) to eμ.

In RPV SUSY, the τ sneutrino signal gives rise to a narrow resonance. For coupling values considered in this analysis, the intrinsic width of this signal is small compared to detector resolution. The Crystal Ball function [33] is therefore used to model the signals. For each probed resonance mass, the two parameters, the product of signal acceptance and efficiency ($A \times \epsilon$) and mass resolution, define the line shape used for limit setting. Both parameters are obtained from fits to MC simulated signal. The parametric forms of $A \times \epsilon$ and mass resolution as a function of signal mass, for the RPV $\tilde{\nu}_\tau$ model are given in Table 1. The values of $A \times \epsilon$ for $\tilde{\nu}_\tau$ events were given in Section 4. The invariant mass resolution ranges from 2.2% at a resonance mass of 200 GeV to 3.1% at 3 TeV. The parametrization of the resonance line shape provides a scan of the invariant mass spectrum with fine binning in signal mass. The QBH signal exhibits a broader distribution with a ledge at the threshold mass m_{th}, which is smeared out by detector resolution, and a tail at larger masses that falls off due to the PDF of the proton. The QBH signals are not parametrized but obtained from the simulated invariant mass distributions. The Z′ signals gives rise to resonance forms that are also directly taken from simulation.

Table 1: Parametrization functions for the acceptance times efficiency and the invariant mass resolution for the RPV signal. The value of $m_{\tilde{\nu}_\tau}$ is given in units of GeV.

Parameter	Functional form
$A \times \epsilon$	$-0.838 + \frac{1.67 \cdot 10^{-2}}{(m_{\tilde{\nu}_\tau}^{-1.02} + 1.0 \cdot 10^{-2})} - 1.54 \cdot 10^{-5} m_{\tilde{\nu}_\tau}$
Mass resolution	$1.79 \cdot 10^{-2} + 1.47 \cdot 10^{-5} m_{\tilde{\nu}_\tau} - 3.87 \cdot 10^{-9} m_{\tilde{\nu}_\tau}^2 + 4.34 \cdot 10^{-13} m_{\tilde{\nu}_\tau}^3$

An upper limit at the 95% confidence level (CL) on the product $\sigma \times B$ is determined using a binned likelihood Bayesian approach [34] assuming a uniform prior for the signal cross section. The signal and background distributions enter the likelihood with a binning of 1 GeV, well below the invariant mass resolution for masses above 200 GeV. The "nuisance" parameters associated with the systematic uncertainties are modelled through log-normal distributions for uncertainties on the normalization or template morphing for the shape uncertainties. A Markov Chain MC method [35] is used for integration. For each mass hypothesis, the posterior probability density function is calculated as a function of $\sigma \times B$ and yields the 95% CL upper limit on this parameter of interest.

The 95% CL limits on $\sigma \times B$ for the RPV $\tilde{\nu}_\tau$ signal are shown in Fig. 2 (left). The signal cross section is calculated at NLO for the RPV couplings $\lambda_{132} = \lambda_{231} = \lambda'_{311} = 0.01$ and 0.1. The factorization and renormalization scales that enter the calculation are set to the mass of the τ

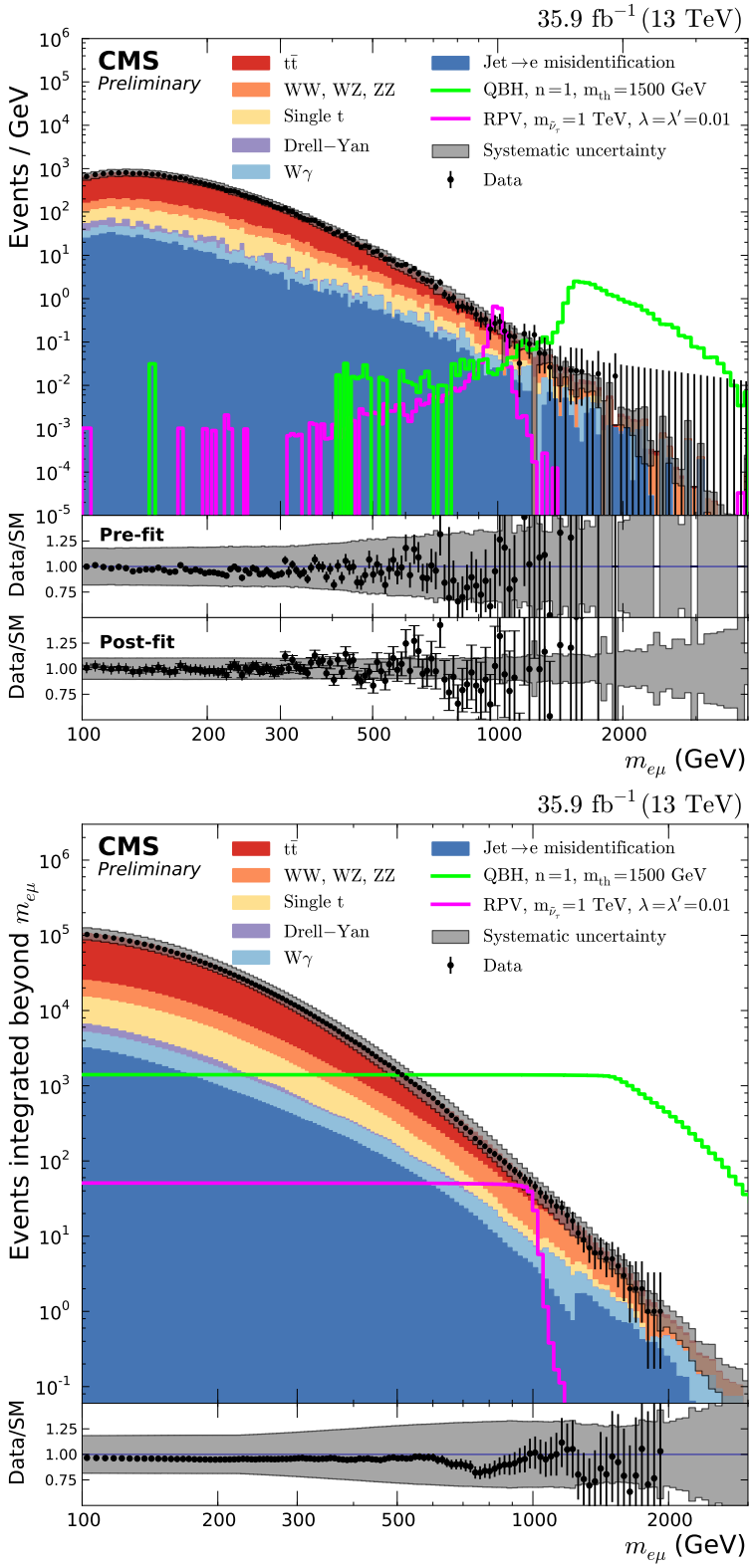

Figure 1: **Upper plot**: The invariant mass distribution of selected eμ pairs. The black points with error bars represent data and the stacked histograms represent the expectations from SM processes. The total systematic uncertainties are shown as a gray band. **Lower plot**: The cumulative (integral) distribution in events integrated beyond the chosen $m_{e\mu}$. Also, expectations are given for several possible signals.

sneutrino. For the couplings of 0.01, a lower mass limit of 1.7 TeV is obtained, while a limit of 1.9 TeV is expected. For RPV couplings $\lambda_{132} = \lambda_{231} = \lambda'_{311} = 0.1$, we observe and expect 3.8 TeV mass limit. In the narrow-width approximation, the $\sigma \times B$ scales with the RPV couplings as [11]:

$$\sigma \times B \approx (\lambda'_{311})^2[(\lambda_{132})^2 + (\lambda_{231})^2]/(3(\lambda'_{311})^2 + [(\lambda_{132})^2 + (\lambda_{231})^2]).$$

Using this relation and the observed upper bounds, we obtain limit contours in the $(m_{\tilde{\nu}_\tau}, \lambda'_{311})$ parameter plane for some fixed values of λ. The result is shown in Fig. 2 (right).

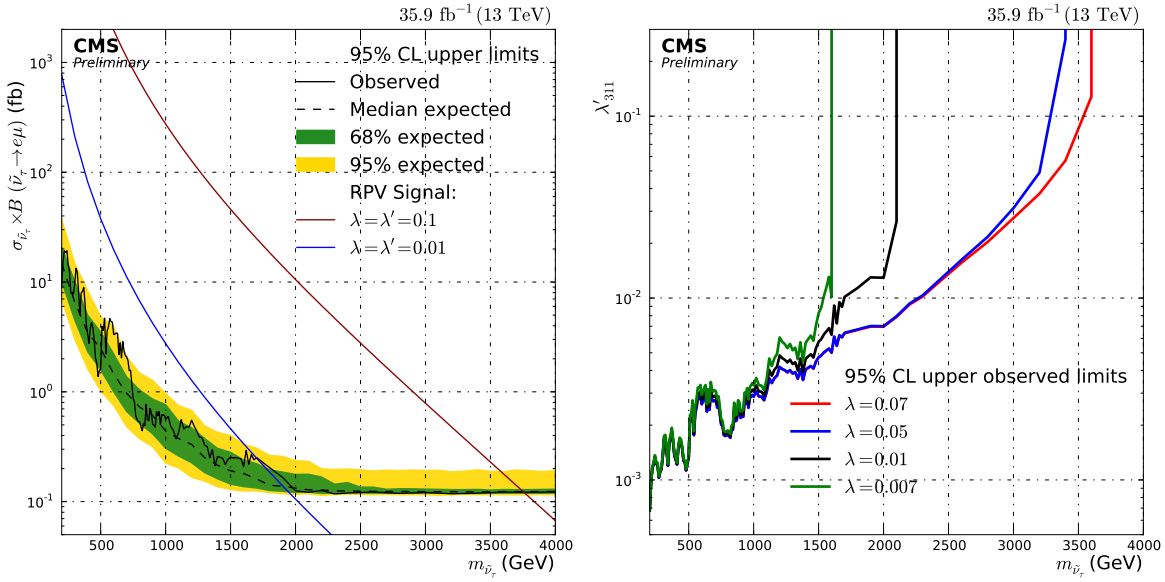

Figure 2: **Left**: 95% CL upper limit on the signal cross section multiplied by branching fraction for the RPV $\tilde{\nu}_\tau$ signal as a function of the mass of the resonance. **Right**: 95% CL limit contours for the RPV $\tilde{\nu}_\tau$ signal in the$(m_{\tilde{\nu}_\tau}, \lambda'_{311})$ parameter plane. The region left and above the limit contour is excluded.

In the QBH search, we set mass limits on the production threshold in models with $n = 1$ (RS) and $n > 1$ (ADD) extra dimensions. The 95% CL limits on $\sigma \times B$ for the QBH signal are shown in Fig. 3. The observed and expected lower mass limits on m_{th} are numerically the same and correspond to 3.6, 5.3, 5.5, and 5.6 TeV for $n = 1$, 2, 3, and 6, respectively. The 95% CL expected and observed limits on the Z′ signal mass are also the same and equal to 4.4 TeV, as shown in Fig. 4.

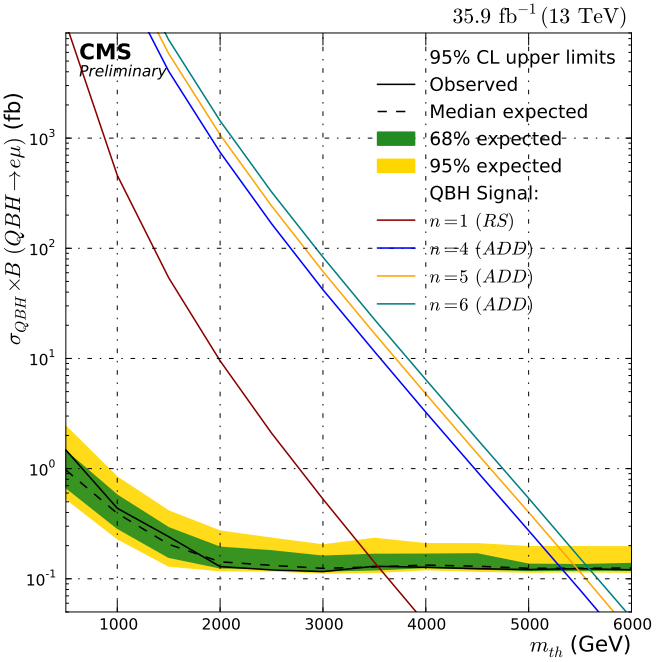

Figure 3: 95% CL upper limit on the median product of the signal cross section and the branching fraction for the QBH signal to eμ as a function of the threshold mass m_{th}.

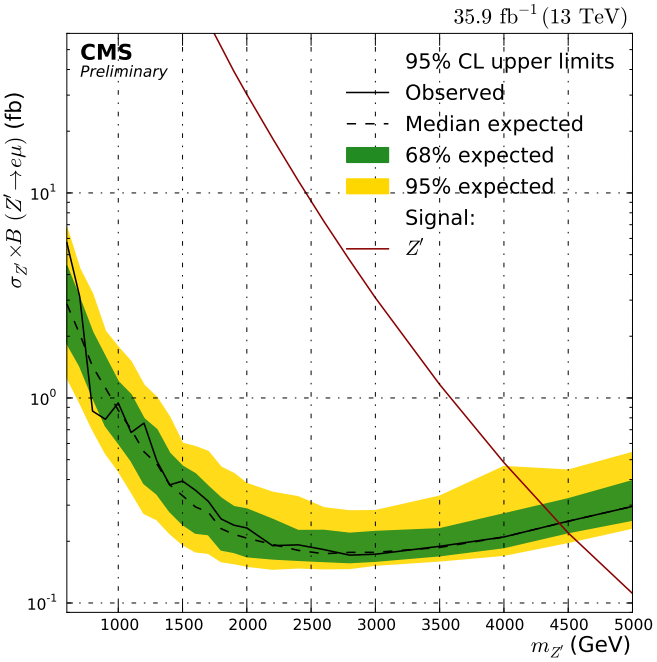

Figure 4: The 95% CL exclusion limit on the product of signal cross section multiplied by the branching fraction of 10 % for the decay into eμ for the Z′ signal as a function of the mass $m_{Z'}$. The observed limit looks smoother than for the RPV signal because of the fewer number of signal mass hypotheses probed for Z′.

8 Summary

A search for heavy resonances decaying into eμ pairs has been carried out using proton-proton collision data recorded with the CMS detector at the LHC at a centre-of-mass energy of 13 TeV and corresponding to an integrated luminosity of 35.9 fb^{-1}. Good agreement is observed between the data and the SM expectation. We set limits on resonant production of τ sneutrinos in R-parity violating supersymmetric (SUSY) models. For couplings $\lambda_{132} = \lambda_{231} = \lambda'_{311} = 0.01$, we exclude τ sneutrino for masses below 1.7 TeV, assuming that it is the lightest supersymmetric particle in these models. For couplings $\lambda_{132} = \lambda_{231} = \lambda'_{311} = 0.1$, we exclude a tau sneutrino lightest SUSY particle for masses below 3.8 TeV. The corresponding expected limits are 1.9 and 3.8 TeV. Also, a Z′ boson with 10 % branching fraction to the eμ channel is excluded for masses below 4.4 TeV. We set lower limits on the threshold mass of quantum black holes in the model with large extra spatial dimensions of 5.3, 5.5, and 5.6 TeV for the number of extra dimensions of 4, 5, and 6, resepctively. For the model with a single, warped extra spatial dimension, the limit is 3.6 TeV. In all cases, the results of this search improve on the previous limits by about 1 TeV.

References

[1] R. Barbier et al., "R-parity violating supersymmetry", *Phys. Rept.* **420** (2005) 1, doi:10.1016/j.physrep.2005.08.006, arXiv:hep-ph/0406039.

[2] P. Langacker, "The Physics of Heavy Z' Gauge Bosons", *Rev. Mod. Phys.* **81** (2009) 1199, doi:10.1103/RevModPhys.81.1199, arXiv:0801.1345.

[3] X. Calmet, W. Gong, and S. D. H. Hsu, "Colorful quantum black holes at the LHC", *Phys. Lett. B* **668** (2008) 20, doi:10.1016/j.physletb.2008.08.011, arXiv:0806.4605.

[4] P. Meade and L. Randall, "Black Holes and Quantum Gravity at the LHC", *JHEP* **05** (2008) 003, doi:10.1088/1126-6708/2008/05/003, arXiv:0708.3017.

[5] D. M. Gingrich, "Quantum black holes with charge, colour, and spin at the LHC", *J. Phys.* **G37** (2010) 105008, doi:10.1088/0954-3899/37/10/105008, arXiv:0912.0826.

[6] L. Randall and R. Sundrum, "A large mass hierarchy from a small extra dimension", *Phys. Rev. Lett.* **83** (1999) 3370, doi:10.1103/PhysRevLett.83.3370, arXiv:hep-ph/9905221.

[7] N. Arkani-Hamed, S. Dimopoulos, and G. R. Dvali, "The hierarchy problem and new dimensions at a millimeter", *Phys. Lett. B* **429** (1998) 263, doi:10.1016/S0370-2693(98)00466-3, arXiv:hep-ph/9803315.

[8] CDF Collaboration, "Search for R-parity Violating Decays of τ sneutrinos to eμ, $\mu\tau$, and eτ Pairs in p$\bar{\text{p}}$ Collisions at $\sqrt{s} = 1.96$ TeV", *Phys. Rev. Lett.* **105** (2010) 191801, doi:10.1103/PhysRevLett.105.191801, arXiv:1004.3042.

[9] D0 Collaboration, "Search for sneutrino production in emu final states in 5.3 fb^{-1} of p$\bar{\text{p}}$ collisions at sqrt(s) = 1.96 TeV", *Phys. Rev. Lett.* **105** (2010) 191802, doi:10.1103/PhysRevLett.105.191802, arXiv:1007.4835.

[10] ATLAS Collaboration, "Search for a Heavy Neutral Particle Decaying to eμ, eτ, or $\mu\tau$ in pp Collisions at $\sqrt{s} = 8$ TeV with the ATLAS Detector", *Phys. Rev. Lett.* **115** (2015) 031801, doi:10.1103/PhysRevLett.115.031801, arXiv:1503.04430.

[11] CMS Collaboration, "Search for lepton flavour violating decays of heavy resonances and quantum black holes to an eμ pair in proton-proton collisions at $\sqrt{s}$ = 8 TeV", *Eur. Phys. J. C* **76** (2016) 317, doi:10.1140/epjc/s10052-016-4149-y, arXiv:1604.05239.

[12] ATLAS Collaboration, "Search for new phenomena in different-flavour high-mass dilepton final states in pp collisions at $\sqrt{s} = 13$ Tev with the ATLAS detector", *Eur. Phys. J. C* **76** (2016) 541, doi:10.1140/epjc/s10052-016-4385-1, arXiv:1607.08079.

[13] CMS Collaboration, "The CMS experiment at the CERN LHC", *JINST* **3** (2008) S08004, doi:10.1088/1748-0221/3/08/S08004.

[14] CMS Collaboration, "The CMS trigger system", *JINST* **12** (2017) P01020, doi:10.1088/1748-0221/12/01/P01020, arXiv:1609.02366.

[15] CMS Collaboration, "Performance of Electron Reconstruction and Selection with the CMS Detector in Proton-Proton Collisions at s = 8 TeV", *JINST* **10** (2015) P06005, doi:10.1088/1748-0221/10/06/P06005, arXiv:1502.02701.

[16] CMS Collaboration, "Performance of CMS muon reconstruction in pp collision events at $\sqrt{s} = 7$ TeV", *JINST* **7** (2012) P10002, doi:10.1088/1748-0221/7/10/P10002, arXiv:1206.4071.

[17] A. Belyaev, N. D. Christensen, and A. Pukhov, "CalcHEP 3.4 for collider physics within and beyond the Standard Model", *Comput. Phys. Commun.* **184** (2013) 1729, doi:10.1016/j.cpc.2013.01.014, arXiv:1207.6082.

[18] D. M. Gingrich, "Monte Carlo event generator for black hole production and decay in proton-proton collisions", *Comput. Phys. Commun.* **181** (2010) 1917, doi:10.1016/j.cpc.2010.07.027, arXiv:0911.5370.

[19] T. Sjöstrand, S. Mrenna, and P. Z. Skands, "A Brief Introduction to PYTHIA 8.1", *Comput. Phys. Commun.* **178** (2008) 852, doi:10.1016/j.cpc.2008.01.036, arXiv:0710.3820.

[20] CMS Collaboration, "Event generator tunes obtained from underlying event and multiparton scattering measurements", *Eur. Phys. J. C* **76** (2016) 155, doi:10.1140/epjc/s10052-016-3988-x, arXiv:1512.00815.

[21] J. Pumplin et al., "New generation of parton distributions with uncertainties from global QCD analysis", *JHEP* **07** (2002) 012, doi:10.1088/1126-6708/2002/07/012, arXiv:hep-ph/0201195.

[22] NNPDF Collaboration, "Parton distributions for the LHC Run II", *JHEP* **04** (2015) 040, doi:10.1007/JHEP04(2015)040, arXiv:1410.8849.

[23] GEANT4 Collaboration, "GEANT4: A simulation toolkit", *Nucl. Instrum. Meth. A* **506** (2003) 250, doi:10.1016/S0168-9002(03)01368-8.

[24] J. Allison et al., "Geant4 developments and applications", *IEEE Trans. Nucl. Sci.* **53** (2006) 270, doi:10.1109/TNS.2006.869826.

[25] J. Allison et al., "Recent developments in geant4", *Nuclear Instruments and Methods in Physics Research Section A: Accelerators, Spectrometers, Detectors and Associated Equipment* **835** (2016) 186, doi:https://doi.org/10.1016/j.nima.2016.06.125.

[26] S. Alioli, P. Nason, C. Oleari, and E. Re, "A general framework for implementing NLO calculations in shower Monte Carlo programs: the POWHEG BOX", *JHEP* **06** (2010) 043, doi:10.1007/JHEP06(2010)043, arXiv:1002.2581.

[27] R. Frederix and S. Frixione, "Merging meets matching in MC@NLO", *JHEP* **12** (2012) 061, doi:10.1007/JHEP12(2012)061, arXiv:1209.6215.

[28] J. Alwall et al., "MadGraph 5: Going Beyond", *JHEP* **06** (2011) 128, doi:10.1007/JHEP06(2011)128, arXiv:1106.0522.

[29] B. D. Pecjak, D. J. Scott, X. Wang, and L. L. Yang, "Resummed differential cross sections for top-quark pairs at the LHC", *Phys. Rev. Lett.* **116** (2016) 202001, doi:10.1103/PhysRevLett.116.202001, arXiv:1601.07020.

[30] CMS Collaboration, "CMS Luminosity Measurements for the 2016 Data Taking Period", CMS Physics Analysis Summary CMS-PAS-LUM-17-001, 2017.

[31] J. Butterworth et al., "PDF4LHC recommendations for LHC Run II", *J. Phys. G* **43** (2016) 023001, doi:10.1088/0954-3899/43/2/023001, arXiv:1510.03865.

[32] R. D. Ball et al., "Parton distributions with LHC data", *Nucl. Phys. B* **867** (2013) 244, doi:10.1016/j.nuclphysb.2012.10.003, arXiv:1207.1303.

[33] M. Oreglia, "A Study of the Reactions $\psi' \to \gamma\gamma\psi$". PhD thesis, SLAC, 1980.

[34] ATLAS, CMS, LHC Higgs Combination Group Collaboration, "Procedure for the LHC Higgs boson search combination in summer 2011", Technical Report ATL-PHYS-PUB-2011-011, CMS-NOTE-2011-005, 2011.

[35] B. C. Allanach and C. G. Lester, "Sampling using a 'bank' of clues", *Comput. Phys. Commun.* **179** (2008) 256, doi:10.1016/j.cpc.2008.02.020, arXiv:0705.0486.